MODERN COMPUTATIONAL METHODS FOR THE DESIGN AND ANALYSIS OF POWER SYSTEM GROUNDING

J. Ma and F. P. Dawalibi

Safe Engineering Services & technologies ltd.
1544 Viel, Montreal, Quebec, Canada, H3M 1G4
Tel.: (514) 336-2511   Fax: (514) 336-6144   E-mail: jinxi@sestech.com

Abstract: *This paper examines a few methods used in grounding analysis and illustrates the advantages, limitations, and the applicability of these methods. Computation results using these methods are presented and compared. The various cases modeled in this paper include grounding networks of different sizes, grounding networks with buried metallic structures such as steel pipes, and high frequency cases. The discussions and conclusions given in this paper can be used as a reference when deciding which method should be used to carry out an accurate and efficient grounding analysis.*

1. Introduction

Appropriate power system grounding is important for maintaining reliable operation of electric power systems, protecting equipment, and insuring the safety of public and personnel. Different computational methods are employed in the analysis and design of power system grounding networks. To carry out an accurate and efficient grounding analysis, it is essential to be aware of the advantages and limitations of the different methods employed. The objective of this paper is to examine a few methods used in grounding analysis and illustrate the advantages, limitations, and the applicability of these methods.

The most commonly used method for grounding analysis is based on the method of images and assumes that the grounding system is an equipotential structure. It gives accurate results for non-extensive grounding networks at low frequencies. Another method takes into account voltage drops along conductors in a grounding network, therefore eliminating the assumption that the grounding system is an equipotential structure. This method, while capable of computing potentials at every point in the grounding system, does not account for the inductive and capacitive interactions between conductors of the grounding system. A third method, which is not commonly used, is based on a field theory approach. Like the second method, it does not require that the grounding system be an equipotential structure. Furthermore, it takes into account not only the self impedances of ground conductors but also the inductive and capacitive interactions between the conductors. For convenience, we shall denote the three methods described above as Approaches 1, 2, and 3, respectively. Interested readers may refer to [1-3] for description of the computer algorithms (MALT, MALZ, and HIFREQ in the CDEGS software package), which are corresponding to the three approaches described above.

Computation results using the methods described above are presented and compared in this paper. The scenarios modeled include grounding networks of different sizes, grounding

networks with buried metallic structures, high frequency cases, and situations in which inductive coupling effects are important.

2. Small Grounding Systems

Figure 1 shows a plan view of a grounding grid with an area of 60 m by 40 m. The conductors constituting the grid are copper with radii of 0.01 m. The grid is buried at a depth of 0.5 m.
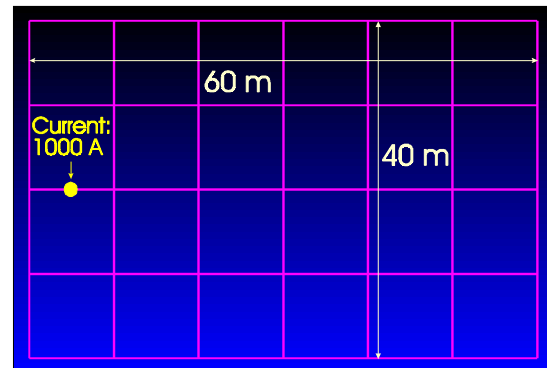

Figure 1.   Plan View of Small Grounding Grid Modeled.

Assuming a 100 Ω-m soil resistivity and a current of 1000 A, the computed GPR (Ground Potential Rise) of the grid at the injection point is 960.4 V using Approach 1 and 960.9 V using Approaches 2 and 3. Obviously, the difference is negligible. The potential magnitudes at different locations in the grounding grid, computed using Approaches 2 and 3, are almost identical: 0.1% difference between the maximum and minimum GPRs. The computed earth surface potentials and the touch voltages using the three different approaches are also identical. In summary, there is no noticeable difference between the results using different approaches for the small grid.

3. Medium-Sized Grounding Systems

Figure 2 shows a 280 m by 140 m grounding grid which is installed in a switchyard area of a substation. The grid consists of copperweld conductors with radii of 0.01m. The numbers labeled besides the ground conductors are the computed potential magnitudes in the grounding grid using Approaches 2 and 3, assuming a soil resistivity of 100 Ω-m and an injection current of 1000 A.

It can be seen that there are differences between the conductor potentials at different locations of the grid, although they are not large. The variation of the conductor potential magnitude throughout the grounding system is within 7%. This implies

that the equipotentiality of the grounding structure is essentially satisfied, suggesting that Approach 1 should give a good approximation. In fact, the potential rise of the grounding system computed using Approach 1 is 253 V, a value between the largest and smallest potential magnitudes (265 V and 248 V) computed using Approaches 2 and 3.

Figure 3 shows the earth surface potentials along the profile shown in Figure 2. The potentials were computed using all three approaches. The differences between the results using different approaches are less than 3%. It can be concluded that for small grounding systems or even medium-sized grounding systems like this one, all three approaches give accurate results. Since the algorithm based on the first approach is simpler and computationally more efficient, it is preferable to use it under these circumstances.
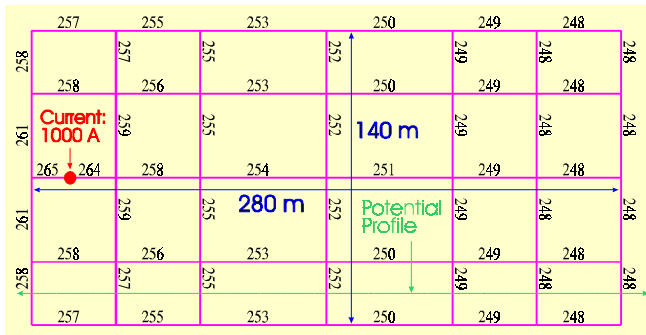

Figure 2. Distribution of the Conductor Potential Magnitudes in the Switchyard Grounding Grid Computed Using Approaches 2 and 3.
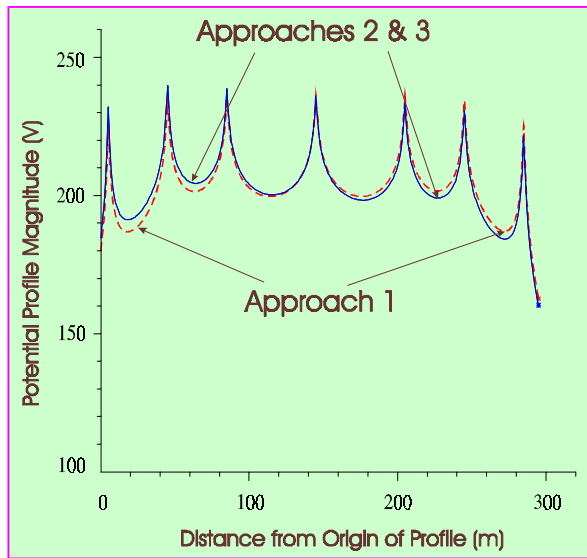

Figure 3. Earth Surface Potentials in the Switchyard Grounding Grid Area.

4. Large Grounding Systems

Let us consider the large grounding system (440 m by 280 m) shown in Figure 4 which includes the switchyard grounding grid shown in Figure 2. The conductor potential magnitudes in the grounding system computed using Approaches 2 and 3 are shown in Figures 4. The difference between the largest

potential magnitude (173 V) and the smallest (139 V) is about 24%. When Approach 1 is used, the computed potentials everywhere in the grounding system are 150 V, a value between the largest and smallest potential magnitudes computed using Approaches 2 and 3, as expected. The ground impedance of the grounding system is 0.150 Ω using Approach 1 and 0.173 Ω using Approaches 2 and 3, giving a 15% difference. It should also be mentioned that the impedance computed using Approaches 2 and 3 has an angle of 13 degrees, implying an inductive component in the impedance which is ignored when Approach 1 is used for computation.

Figure 5 shows the earth surface potentials computed along the profile shown in Figure 5 based on all three approaches. It can be seen that the earth potentials computed using Approaches 2 and 3 are practically identical. The earth potentials computed using Approach 1 are lower at locations close to the injection point and higher away from it. The overall difference is not very large (on the order of 6%) even for this large grid.
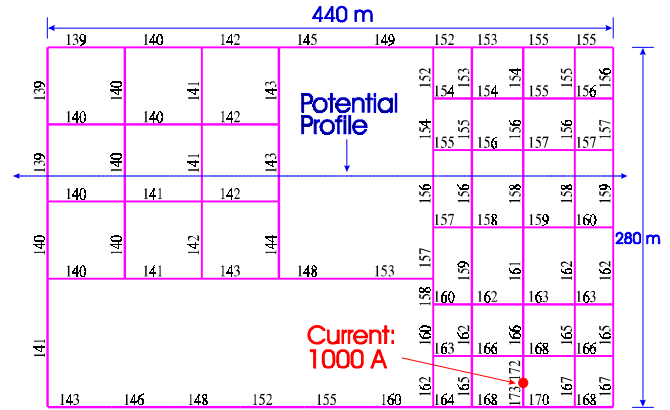

Figure 4. Distribution of the Conductor Potential Magnitudes in the Substation Grounding Grid Computed Using Approaches 2 and 3.
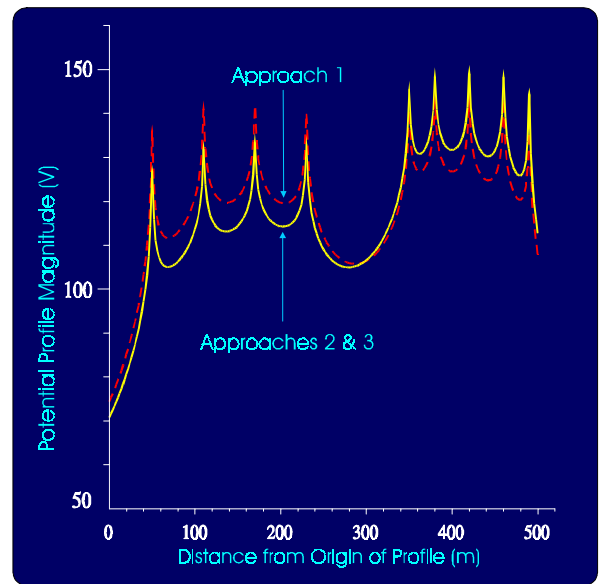

Figure 5. Earth Surface Potentials in the Substation Area.

5. Grounding Systems with Different Conductor Characteristics

If steel conductors are used instead of copperweld conductors in the grounding grid shown in Figure 4, the difference between the results obtained using different approaches can be significant. Figure 6 shows the conductor potential magnitudes in the grounding system computed using Approaches 2 and 3. The difference between the largest potential magnitude (257 V) and smallest (106 V) is now more than 140% compared with 24% in Figure 4. Since Approach 1 assumes equipotentiality of the grid, the conductor characteristics are not taken into account in the computation. Hence the computed potentials everywhere in the grounding system are 150 V using Approach 1. This value is still between the largest and smallest potential magnitudes shown in Figure 6, computed using Approaches 2 and 3. In this case, the ground impedance of the grounding system is 0.150 Ω using Approach 1 and 0.257 Ω using Approaches 2 and 3, giving a difference of more than 70%. Note also that the impedance computed using Approaches 2 and 3 has an angle of 15 degrees, implying an inductive component on the order of 27% of the resistive part.

For the purpose of comparison, we have also computed the ground impedances for the small and medium-sized grids consisting of steel conductors. The ground impedance is 0.965 Ω for the small grid and 0.335 Ω for the medium-sized grid, compared with 0.961 Ω and 0.265 Ω with copper conductors for the small grid and copperweld conductors for the medium-sized grid, respectively. We can see that for the small grid, the influence of the conductor characteristics is negligible, while for the medium-sized grid, the effect is already significant.
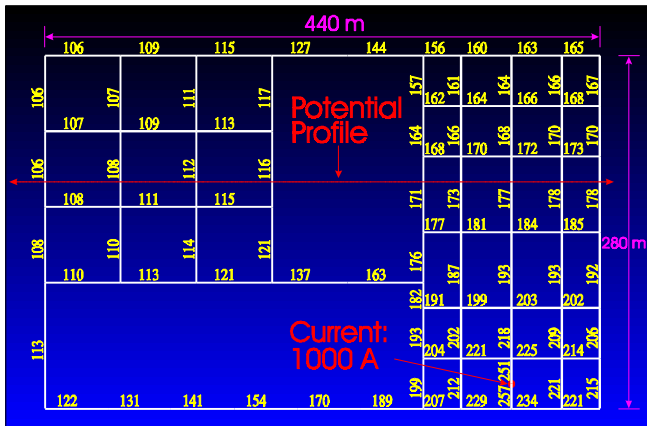

Figure 6. Distribution of the Conductor Potential Magnitudes in the Substation Grounding Grid Made of Steel Conductors Computed Using Approaches 2 and 3.

Figure 7 shows the earth surface potentials computed along the profile based on all three approaches. Again the results obtained using Approaches 2 and 3 are almost identical. However, the results obtained using Approach 1 are quite different from those using Approaches 2 and 3. The difference is on the order of 33%.
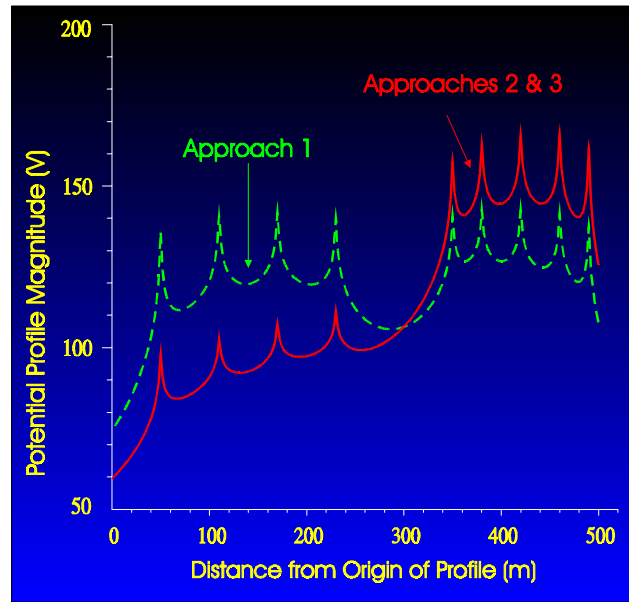

Figure 7. Earth Surface Potentials in the Substation Area (Grid with Steel Conductors).

One practical example of a grounding system with different conductor characteristics is a grounding grid connected to buried metallic pipes and steel rebars in building foundations. In this case, Approach 1 will not give accurate results. Figure 8 shows an example of a grounding grid connected to the steel rebars of a building foundation by a buried steel pipe. The distribution of potentials along the conductors is also shown in this figure. The potential gradually drops along the pipe. At the location of the steel rebars, the potential is 30% lower than the grid GPR (288 V compared with 413 V). Figure 9 shows the earth surface potentials computed along the profile based on all three approaches. The difference is significant between the Approach 1 results and those obtained using Approaches 2 and 3. It should be pointed out that when a substation is in an urban area, the grounding system of the substation is usually directly or indirectly connected to the underground pipe network. In this case, the evaluation of the ground impedance has to be carried out using Approach 2 or 3. If the pipe network is ignored, the computed ground impedance is too high compared to the true ground impedance. On the other hand, when the pipe network is modeled, the computed ground impedance can be substantially lower than the true value if Approach 1 is used for the calculation.
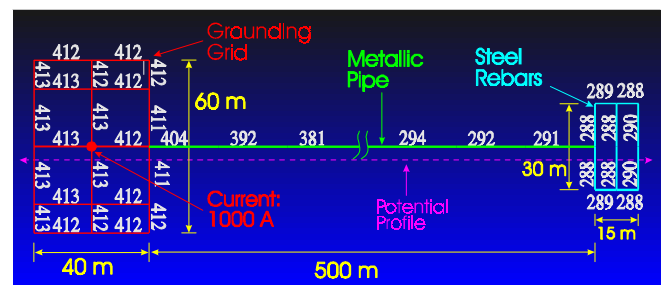

Figure 8. Distribution of Conductor Potential Magnitudes in the Grounding Grid, Pipe, and Steel Rebars.
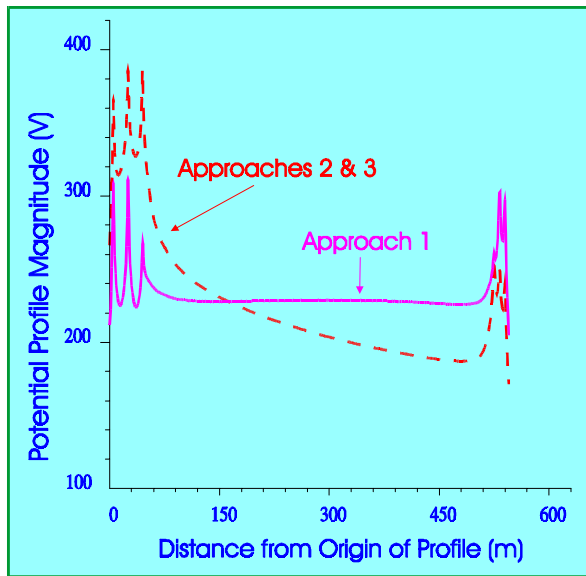
Figure 9. Earth Surface Potentials along the Metallic Pipe Interconnecting the Grounding Grid and the Steel Rebars.

6. Circulating Currents in Grounding Grids

During a fault on the secondary side of a transformer located in a substation, considerable circulating currents can flow through the grounding system from the fault location to the transformer feeding the fault, resulting in large potential differences between different locations of the grid. Non-grounded conductors, such as control or communications wires, connected to equipment at two such parts of the grid, may be subjected to potential differences (stress voltages) between the equipment connections and the grounding grid, resulting in possible damage to the equipment. To carry out such a study, Approach 1 cannot be used due to the equipotentiality assumption. Both approaches 2 and 3 can be used while Approach 3 is usually preferred when aboveground structures need to be modeled. This is because Approach 2 ignores the inductive and capacitive interactions between the conductors, which may be significant for aboveground structures. Figure 10 shows such a fault scenario for the substation grounding grid shown in Figure 4. A total fault current of 38 kA is injected into the grounding grid at Point A. At Point B, corresponding to the neutral bonding point of the star secondary windings of a transformer, 24.6 kA is collected. The difference between the injected and collected fault currents (13.4 kA), supplied via incoming transmission lines, returns to remote power supply sources through the earth. The circulating current in the grid is shown in Figure 10, computed using Approach 2. It can be seen that there are large circulating currents flowing through the grounding grid, which cause the large potential differences between different locations of the grounding system. The GPRs at Points A and B are 3594<30^0 V and 1863<-52^0 V, respectively. When Approach 3 is used, they are 3657<27^0 V and 1978<-54^0 V, respectively. Obviously, the potential difference in the grounding grid computed using Approach 3 is larger than that computed using Approach 2. This is because Approach 3 takes into account the inductive coupling between the ground

conductors and as such, the impedances along the path from A to B are larger.

When a fault occurs on the primary side of a transformer, most of the fault current is discharged through the grounding system and returns to the remote source. This case corresponds to the one injection point scenario. In this case, the GPR of the grid can be high, but the potential differences in the grid are low because the average current flowing through the grid is smaller.
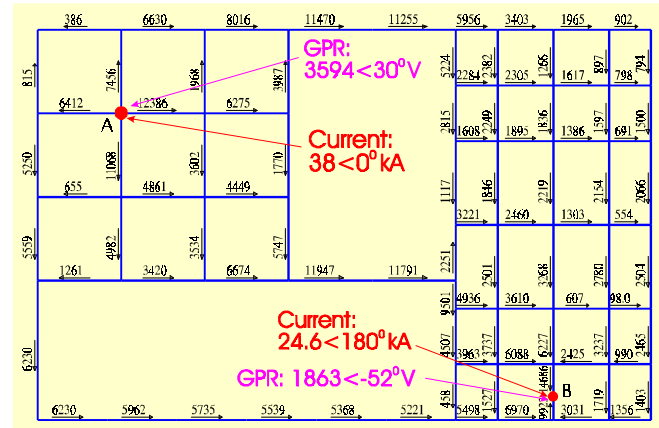

Figure 10. Circulating Currents in the Grounding Grid.

7. High Frequency Cases

It is often necessary to evaluate the frequency response of a grounding system in dealing with problems related to lightning or capacitor bank switching transients. In this case, only Approaches 2 and 3 can be used. Moreover, for very high frequencies, even Approach 2 is inadequate because it does not account for the inductive and capacitive coupling between conductors. Let us consider the small grounding grid shown in Figure 1 for high frequency cases. Figure 11 shows a 3D plot of the earth surface potentials in the grid area at 60 Hz, computed using Approach 3. At this low frequency, the results obtained using all approaches are very close.
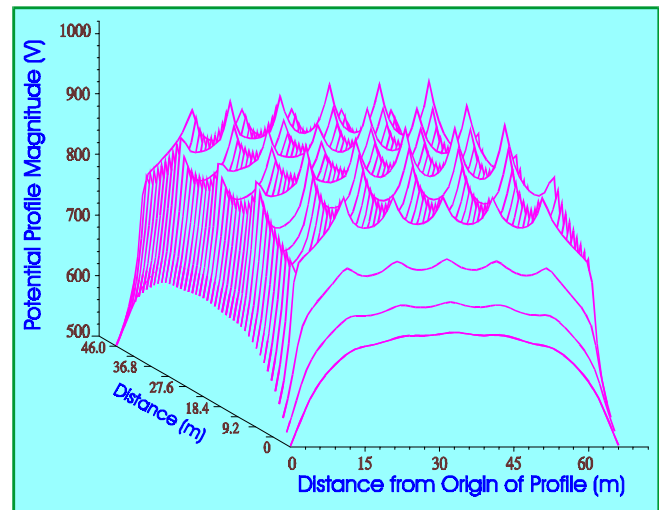

Figure 11. Earth Surface Potentials over the Small Grounding Grid at 60 Hz.

The earth surface potentials, computed using Approach 3 at 50 kHz and 1 MHz, are shown in Figures 12 and 13, respectively. It can be seen that at locations close to the injection point, the potentials are very high. Away from the injection point, the potentials decrease very rapidly. In the 60 Hz case, the injection point location has almost no influence. As the frequency increases, the effective area of the grid decreases, resulting in a large ground impedance value. At 50 kHz, the ground impedance is $2.8 < 45^0$ Ω, and at 1 MHz, it is $15.6 < 43^0$ Ω, compared with 0.96 Ω at 60 Hz. The differences between the ground impedance values computed using Approaches 2 and 3 are 10% at 50 kHz and 13% at 1 MHz.
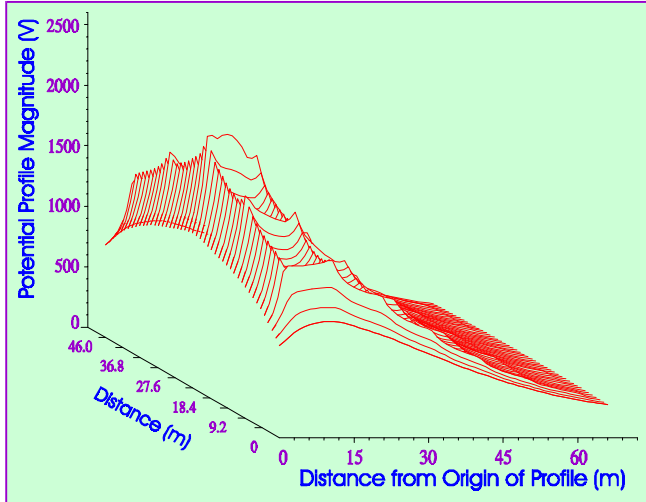

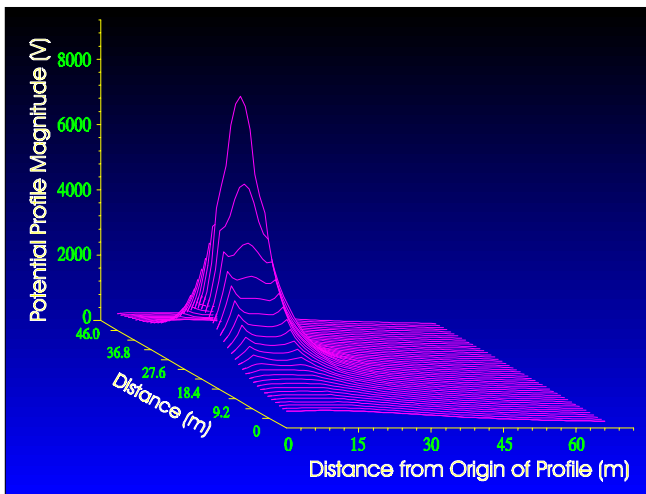Figure 12. Earth Surface Potentials over the Small Grounding Grid at 50 kHz.

Figure 13. Earth Surface Potentials over the Small Grounding Grid at 1 MHz.

8. Aboveground Structure Modeling

It is sometimes necessary to model aboveground structures together with the grounding system, in order to compute surge impedances of towers, study the influence of inductive coupling on soil resistivity measurements and on ground impedance measurements, or analyze inductive interference between power lines and pipelines which share the same corridor. In this case, only Approach 3 can be used because other approaches do not take into account the inductive and capacitive coupling between conductors. Figure 14 shows a practical setup for the measurement of ground impedance using the Fall-of-Potential Method. Figure 15 shows the Fall-of-Potential curves corresponding to the case without inductive coupling, and two cases with 1 m and 10 m separation distances between the current and potential leads. In a uniform soil, at the potential probe location, X=618 m, the true ground impedance, 0.523 Ω, is measured. Due to inductive coupling, the measured ground impedance becomes 0.601 Ω for the 10 m separation distance between the current and potential leads, and 0.668 Ω for the 1 m separation distance, representing a 15% and 28% error, respectively. When the frequency is higher, the inductive coupling can be much stronger. In this example, the case without coupling can be analyzed using any of the three approaches, while the case with coupling can be analyzed using Approach 3.
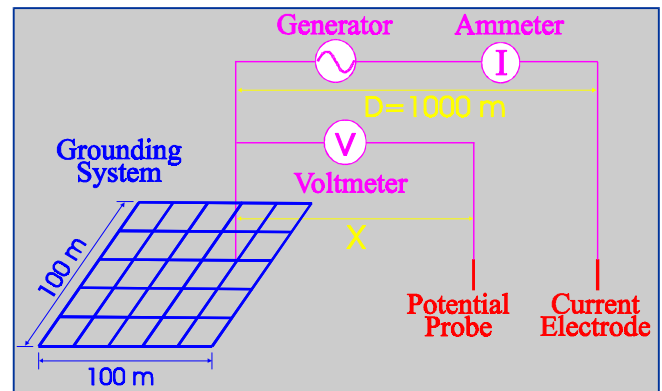

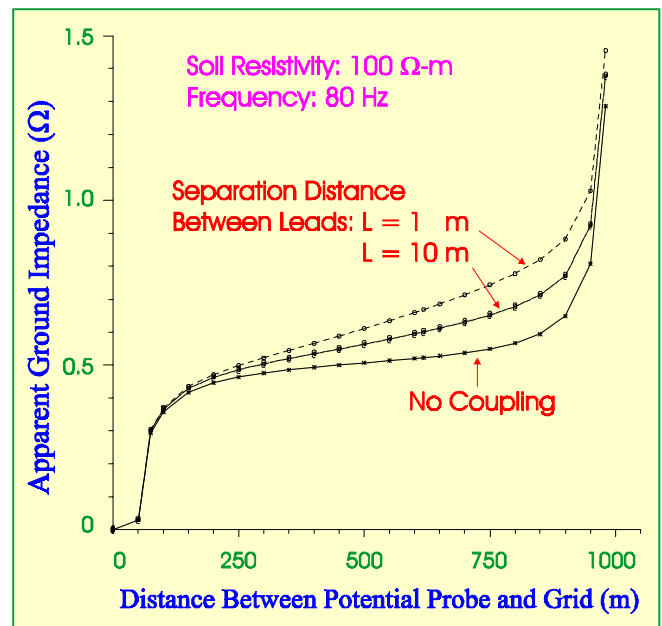Figure 14. Ground Impedance Measurement Setup.

Figure 15. Computed Fall-of-Potential Measurement Curves.

9. Conclusions

Three methods used in grounding analysis have been examined. Computation results using these methods have been presented and compared for grounding networks of different sizes, grounding networks with buried metallic structures such as steel pipes and rebars, high frequency cases, and inductive coupling effect evaluations. It is shown that the commonly used grounding analysis algorithm with the assumption of equipotentiality of grounding systems gives satisfactory results for small and medium-sized grounding grids consisting of copper conductors. However, for large grounding networks consisting of steel conductors such as water pipes, the computation of grid potential differences and the evaluation of the high frequency performance of grounding grids, require adequate approaches such as Approaches 2 and 3 described in this paper. For very high frequency cases or for modeling aboveground structures, Approach 3 should be used to adequately account for the inductive and capacitive coupling between conductors. It should be pointed out that Approach 1 is more computationally efficient than Approach 2 and that Approach 2 is more computationally efficient than Approach 3. On the other hand, Approach 3 is the most general and accurate method and hence can be used to model most enigization problems from 0 to the gigahertz range while Approach 2 has a broader applicability than Approach 1 but both are confined to buried structures.

10. References

[1] F.P. Dawalibi and F. Donoso, "Integrated Analysis Software for Grounding, EMF, and EMI", IEEE Computer Applications in Power, 1993, Vol. 6, No. 2, pp. 19-24.

[2] J. Ma and F.P. Dawalibi, "Hazardous potential differences in extensive grounding systems during ground faults", 58th Annual Meeting of the American Power Conference, Chicago, April 1996.

[3] F.P. Dawalibi, W. Xiong, and J. Ma, "Transient Performance of Substation Structures and Associated Grounding Systems", IEEE Transactions on Industry Applications, Vol. 31, No. 3, May/June 1995, pp. 520-527.

11. BIOGRAPHY

Dr. Jinxi Ma was born in Shandong, P.R. China in December 1956. He received the B.Sc. degree in radioelectronics from Shandong University, and the M.Sc. degree in electrical engineering from Beijing University of Aeronautics and Astronautics, in 1982 and 1984, respectively. He received the Ph.D. degree in electrical and computer engineering from the University of Manitoba, Winnipeg, Canada in 1991. From 1984 to 1986, he was a faculty member with the Dept. of Electrical Engineering, Beijing University of Aeronautics and Astronautics. He worked on projects involving design and analysis of reflector antennas and calculations of radar cross sections of aircraft.

Since September 1990, he has been with the R & D Dept. of Safe Engineering Services & Technologies in Montreal, where he is presently serving as manager of the Analytical R & D Department. His research interests are in transient electromagnetic scattering, EMI and EMC, and analysis of grounding systems in various soil structures.

Dr. Ma has authored and coauthored more than fifty papers on transient electromagnetic scattering, analysis and design of reflector antennas, power system grounding, lightning and electromagnetic interference analysis. He is a corresponding member of the IEEE Substations Committee and is active on Working Groups D7 and D9.

Dr. Farid P. Dawalibi (M'72, SM'82) was born in Lebanon in November 1947. He received a Bachelor of Engineering degree from St. Joseph's University, affiliated with the University of Lyon, and the M.Sc. and Ph.D. degrees from Ecole Polytechnique of the University of Montreal. From 1971 to 1976, he worked as a consulting engineer with the Shawinigan Engineering Company, in Montreal. He worked on numerous projects involving power system analysis and design, railway electrific ation studies and specialized computer software code development. In 1976, he joined Montel-Sprecher & Schuh, a manufacturer of high voltage equipment in Montreal, as Manager of Technical Services and was involved in power system design, equipment selection and testing for systems ranging from a few to several hundred kV.

In 1979, he founded Safe Engineering Services & Technologies, a company which specializes in soil effects on power networks. Since then he has been responsible for the engineering activities of the company including the development of computer software related to power system applications.

He is the author of more than one hundred papers on power system grounding, lightning, inductive interference and electromagnetic field analysis. He has written several research reports for CEA and EPRI.

Dr. Dawalibi is a corresponding member of various IEEE Committee Working Groups, and a senior member of the IEEE Power Engineering Society and the Canadian Society for Electrical Engineering. He is a registered Engineer in the Province of Quebec.